Detailed Balance Analysis of Photovoltaic Windows

Lance M. Wheeler[1] and Vincent M. Wheeler[2]

[1]National Renewable Energy Laboratory, 15013 Denver W Pkwy, Golden, CO 80401
[2]University of Wisconsin – Stout, 712 Broadway St S, Menomonie, WI 54751

Abstract

There are a number of technical and socio-economic factors converging to position photovoltaic (PV) windows as a transformative technology for the energy landscape of the future: 1) Urban areas currently account for 67–76% of global final energy consumption. 2) 70% of the world's population will live in urban areas by 2050. 3) The overwhelming architectural trend is away from opaque building components and toward all-glass facades. 4) Photovoltaics are becoming extremely affordable, and the most expensive components in a conventional module are the glass and transparent metals—components that are already in highly-insulating glazing. 5) Buildings are increasingly built to easily integrate with photovoltaic energy generation using DC microgrids and on-site energy generation to balance high demand on the grid. Rational design of PV windows is of paramount importance to realize their impact. In this work, we provide an analysis on the theoretical performance of PV windows using a detailed balance model to understand the complex design space of power conversion efficiency, visible light transmittance, solar heat gain coefficient, and color. We find there are two distinct regimes for PV window absorber design. The first low-visible light transmittance regime validates the most prevalent approach to semitransparent PV windows in which conventional absorber materials (Si, CIGS, CdTe, CZTS, perovskite, etc.) are thinned to allow visible light to pass through. In this thinned-absorber regime, an ideal bandgap of ~1.35 eV maximizes performance, which is consistent with the famous Shockley–Queisser limit. However, we identify a second, high visible light transmittance regime in which the ideal bandgap for maximum power conversion efficiency increases monotonically from 2 to 3 eV with increasing visible light transmittance. In this tuned-bandgap regime, the solar cell exhibits lower losses and tunable solar heat gain and color.

Urban areas currently account for 67–76% of global final energy consumption[1]. With urban living expected to increase from roughly half of the world's population to 70% by the middle of this century[2], energy generation and efficiency in the urban built environment is critical to a sustainable energy future[3]. Though building-integrated photovoltaics (BIPV) have been in development for many decades[4], the rapid decrease in the cost of PV in the past decade makes BIPV an economically tractable direction for on-site energy generation in next-generation buildings[5].

The architectural trend away from conventional opaque materials and toward all-glass building façades[6] makes window-integrated PV the most promising approach to BIPV in the urban environment of the future. Unlike conventional PV technologies that seek to maximize light absorption for high solar-to-electrical power conversion efficiency (PCE), PV windows must reconcile high PCE with high visible light transmittance (VLT), controlled solar heat gain coefficient ($SHGC$), and aesthetically acceptable color[7].

This challenging balancing act has led to PV window designs that may be subdivided into two main categories: (1) Transparent (also called wavelength-selective[8]) designs target the ultraviolet (UV) or infrared (IR) regions of the solar spectrum. UV absorbers target a region that is deficient in photons, which severely limits PCE compared to absorbers optimized to the solar spectrum. IR absorbers target a region that is rich in photons with high theoretical PCE[9,10] but have only demonstrated experimental PCE no greater than 5%[11]. IR absorbers are composed of complex organic semiconductor materials and are limited by the synthetic challenge of producing materials with a molecular absorption profile that is tuned for strong IR absorption and minimal visible light absorption[12]. (2) Semitransparent designs are more prevalent in the literature.[13,14] Designs span patterned opaque PV elements that allow light through between the elements to luminescent solar concentrator schemes in which chromophores, such as quantum dots[15], absorb light in index-matched thin films on glass that waveguide and reemit photons to the window edge where they are converted by conventional PV cells. The most common configuration is the application of thinned absorbers. These schemes tend to have a higher PCE than the transparent designs by converting the photon-rich visible portion of the spectrum, but this is achieved with a direct tradeoff for VLT and added color.

It is critical to the development and practical deployment of PV windows to understand the tradeoffs that shape the complex design space. Though a number of theoretical treatments exist[9,10,12,16], a model that reconciles the complete picture of the PV window parameter space does not. Here we develop a detailed balance model that includes analysis of PCE, VLT, $SHGC$, and color. We identify two distinct regimes for PV window absorber design. The first low-VLT regime ($VLT \leq 0.3$) validates the common approach to semitransparent PV window in which conventional absorber materials (Si, CIGS, CdTe, CZTS, perovskite, etc.) are thinned or patterned to allow visible light to pass through. In this thinned-absorber regime, an ideal bandgap of ~1.35 eV maximizes performance, which is consistent with the Shockley–Queisser (S–Q) limit[17]. We identify a second high-VLT regime ($VLT > 0.3$) in which the ideal bandgap for maximum PCE increases monotonically from 2 to 3 eV with increasing VLT. In this tuned-bandgap regime, the solar cell exhibits lower losses, higher $SHGC$, and color that trends from yellow to orange and red.

PV Window Model

In 1961, Shockley and Queisser introduced the detailed balance model to calculate the maximum theoretical efficiency of a p–n junction solar cell (Fig. 1a)[17]. PCE is

determined using only the absorber bandgap, solar cell temperature, and incoming solar power flux (Q_{Inc}). The model applies simple assumptions: (*i*) All photons above the band gap (E_{Gap}) are absorbed (step function absorption profile). (*ii*) Excited carriers thermalize to the band edge and are either collected as converted power (Q_{Conv}) or radiatively recombined (radiative limit). Thermalization and radiated power contribute to power lost in the cell (Q_{Loss}). (*iii*) The cell temperature (T_{Cell}) remains constant, even with thermalization of carriers.

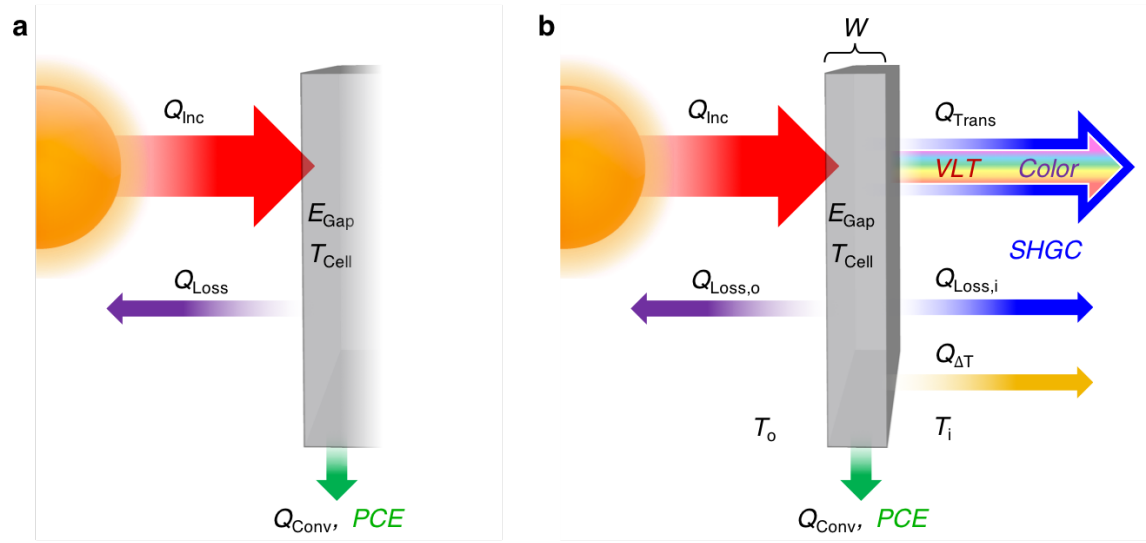

Figure 1. a) Diagram illustrating Shockley–Queisser detailed balance model[17]. **b**) Detailed balance model developed here highlighting the important metrics for PV window performance (PCE, VLT, SHGC, and color)

The S–Q detailed balance model is easily modified to capture different photovoltaic schemes such as tandem cells[15,16], intermediate band cells[18], nanostructured cells[19], thermophotovoltaics[20], photon recycling[21], and absorbers that undergo multiple exciton generation or singlet fission[22]. The maximum theoretical efficiency of transparent and semitransparent absorbers has been modeled by Lunt by assuming a step-function cut-off before and after the visible portion of the spectrum to simulate an idealized excitonic absorption of a molecular absorber[9].

In this work, we first modify the S–Q model to allow T_{Cell} to be a free variable to enable the thermal analysis of the PV window. Figure 1 shows the power transport mechanisms in the S–Q model (Fig. 1a) along with our additional considerations unique to a PV window (Fig. 1b). A statement of conservation of energy at steady state for a unit surface of PV window yields

$$Q_{\mathrm{Abs}} - Q_{Loss,\mathrm{i}} - Q_{\mathrm{Loss,o}} - Q_{\mathrm{Conv}} = 0, \qquad (1)$$

where $Q_{\mathrm{Abs}} = Q_{\mathrm{Abs}}(T_{\mathrm{Cell}})$ is the absorbed solar power; $Q_{\mathrm{Loss,i}} = Q_{\mathrm{Loss,i}}(T_{\mathrm{Cell}})$ and $Q_{\mathrm{Loss,o}} = Q_{\mathrm{Loss,o}}(T_{\mathrm{Cell}})$ are the powers lost to the interior and exterior of the building by convection and thermal radiative emission, respectively.

The absorbed power is calculated using

$$Q_{\mathrm{Abs}} = \int \Gamma\, \eta\; dE, \tag{2}$$

where the solar spectrum is represented by $\Gamma = \Gamma(E)$ and assuming one pass of sunlight through the device with an external quantum efficiency of $\eta = \eta(E, T_{\mathrm{Cell}}) = 1 - \exp(-\alpha W)$. Note that this definition assumes no reflection at the surface of the window. W is the thickness of the absorber layer and $\alpha = \alpha(E, T_{\mathrm{Cell}})$ is the absorption coefficient.

The second modification to the S–Q model is the use of an absorption profile that is not an ideal step-function. We choose a square-root absorption profile characteristic of a direct bandgap semiconductor rather than a molecular absorber,

$$\alpha = \begin{cases} \beta \left(\dfrac{E - E_{\mathrm{Gap}}}{k T_{\mathrm{Cell}}} \right)^{1/2}, & E \geq E_{BG} \\ 0, & E < E_{BG.} \end{cases} \tag{3}$$

where E_{Gap} is the absorber bandgap, k is Boltzmann's constant, E is the photon energy, and β is a constant to be fit to a particular absorber profile (Fig. S1).

The power lost from the window by way of conduction, convection, and thermal emission is calculated from:

$$\begin{aligned} Q_{\mathrm{Loss,i}} &= U_{\mathrm{i}}(T_{\mathrm{Cell}} - T_{\mathrm{i}}), \\ Q_{\mathrm{Loss,o}} &= U_{\mathrm{o}}(T_{\mathrm{Cell}} - T_{\mathrm{o}}). \end{aligned} \tag{4}$$

The power lost to the indoors, $Q_{\mathrm{Loss,i}}$, is determined by the overall heat transfer coefficient, U_i, between the absorber and the indoor air at temperature T_{i}. Power lost to the outdoor air follows analogously. The PV absorber has been assumed to be isothermal—a reasonable assumption for a very thin absorber.

The converted power, Q_{Conv}, is calculated numerically by maximizing the current–voltage product, where the current is determined by the number of electron–hole pairs generated that do not radiatively recombine exactly as described by the original S–Q model[17].

The temperature of the solar cell, T_{Cell}, can now be determined by numerically solving Eq. 1 with Eqs. 2–4 for a set of parameters: β, U_{i}, U_{o}, T_{i}, T_{o}, E_{Gap}, and W. PCE, VLT, $SHGC$, and color can then be determined as summarized in Table 1.

For future analyses, it will be convenient to define the power loss as the difference between the absorbed power and power converted to electricity, $Q_{\mathrm{Loss}} = Q_{\mathrm{Abs}} - Q_{\mathrm{Conv}} = Q_{\mathrm{Loss,i}} + Q_{\mathrm{Loss,o}}$, and to note that the absorbed power summed with the power transmitted through the PV window, Q_{Trans}, must be equal to the incident power $Q_{\mathrm{Inc}} = \int \Gamma \, \mathrm{d}E$,

$$Q_{\mathrm{Abs}} = Q_{\mathrm{Inc}} - Q_{\mathrm{Trans}}. \tag{5}$$

Combining Eqs. 1 and 5 and dividing by Q_{Inc} gives a statement of energy conservation as a set of normalized powers that must equal one:

$$PCE + \frac{Q_{\mathrm{Loss}}}{Q_{\mathrm{Inc}}} + \frac{Q_{\mathrm{Trans}}}{Q_{\mathrm{Inc}}} = 1. \tag{6}$$

Alternatively, Eq. 6 may be rewritten using the definition of $SHGC$ (Table 1):

$$PCE + SHGC + \frac{Q_{\mathrm{Loss,o}} + Q_{\Delta \mathrm{T}}}{Q_{\mathrm{Inc}}} = 1. \quad (7)$$

In our analysis, we used spectral solar irradiance data from the air mass 1.5 ASTM G173 terrestrial reference spectra. The parameter appearing in Eq. 4 has been determined by matching α to the absorption coefficient of a model direct bandgap absorber, $\beta = 1.5 \times 10^{-3}$ nm^{-1}. We chose methylammonium lead iodide due to its popularity in the literature for PV windows[8]. Ellipsometry measurements were performed on single crystals (Fig. S1). The window unit is assumed to provide no thermal resistance, and the overall heat transfer coefficients are assumed to be $U_{\mathrm{i}} = 8.3$ W m^{-2} K^{-1} and $U_{\mathrm{o}} = 17$ W m^{-2} K^{-1} throughout this work based on conventional literature assumptions[23]. A window unit with no thermal resistance is obviously unrealistic for modern, high thermal efficiency windows with multiple glazing. However, the important findings of this work will be unaffected by this assumption and can be easily altered in future work; further discussion will follow with the results. The indoor temperature is set to be T_{i} = 298 K. We investigate three outdoor temperature conditions to reflect fall/spring (T_{o} = 298 K), summer (T_{o} = 311 K), and winter (T_{o} = 273 K). The bandgap energy and absorber thickness are parameters that will be explored.

Table 1: PV window metrics and their meaning.

PV window metric definition	Meaning
$PCE = \frac{Q_{\mathrm{Conv}}}{Q_{\mathrm{Inc}}}$	The PCE is the fraction of incident solar power that is converted to electrical power.
$VLT = \frac{\int \Gamma\,(1-\eta)\,\varphi\; dE}{\int \Gamma\varphi\; dE}$	The VLT is determined by the number of photons transmitted through window weighted by the sensitivity of the human eye to see those photons, which we define as the CIE photopic luminosity function, $\varphi = \varphi(E)$[24] (Fig. S2). This value is divided by the total incident intensity weighted by φ and integrated over the total solar spectrum giving values between zero and one.
$SHGC = \frac{Q_{\mathrm{Trans}} + Q_{\mathrm{Loss,i}} - Q_{\Delta \mathrm{T}}}{Q_{\mathrm{Inc}}}$	The $SHGC$ is the sum of the transmitted power and the power lost in the cell that is transferred to the inside of the building due to a temperature difference between the absorber layer and the indoor air. Heat transfer only due to a temperature gradient is subtracted from the $SHGC$ since it is not part of its definition but has been included in the model to calculate the equilibrium operating temperature of the solar cell: $Q_{\Delta \mathrm{T}} = (T_{\mathrm{o}} - T_{\mathrm{i}})/R_{\mathrm{Tot}}$, where R_{Tot} is the total thermal resistance of the PV window when there is no absorption.
$x = \frac{X}{X+Y+Z}$, $y = \frac{Y}{X+Y+Z}$	Color is determined by the CIE 1931 color space. CIE x and y chromaticity coordinates are determining from the tristimulus values X,Y, Z: $X = \int Q_{\mathrm{Trans}}(E)\,\bar{x}(E)\,\mathrm{d}E$, $Y = \int Q_{\mathrm{Trans}}(E)\,\bar{y}(E)\,\mathrm{d}E$, $Z = \int Q_{\mathrm{Trans}}(E)\,\bar{z}(E)\,\mathrm{d}E$, where $\bar{x}(E)$, $\bar{y}(E)$, and $\bar{z}(E)$ are the color matching functions of the CIE standard colorimetric observer (Fig. S3).

Balancing PCE, VLT, $SHGC$, and Color

The most common metric reported in PV window literature is PCE at a given VLT. PCE versus VLT data from the literature are nicely compiled in a recent work by Lunt and Coworkers[8]. Reported values range widely from PCE = 16.5% at VLT = 0.05 for a semitransparent perovskite cell[25] to PCE = 0.4% at VLT = 0.86 for a near-infrared luminescent concentrator architecture[26]. In this work, a contour plot of PCE as a function of thickness and bandgap for fall/spring conditions (Fig. 2a) shows a maximum PCE of 33.0% at a bandgap of 1.35 eV for thicknesses >800 nm, which is consistent with typical S–Q analysis. Contours calculating PCE for summer (Fig. S4) or winter (Fig. S5) show similar trends with a maximum PCE of 32.6% and 33.7%, respectively. The optimal thickness of the absorber was calculated to obtain maximum PCE for a constant VLT as a function of bandgap (Fig. S6). Lines of constant VLT for VLT = 0.1, 0.5, and 0.9 at maximum PCE are shown as dashed lines overlaying the contours in Fig. 2a. The maximum PCE as a function of bandgap for constant VLT is extracted from the contour, and the result is presented in Fig. 2b for winter (thick lines), fall/spring (dashed lines), and summer (thin lines). Intuitively, the outdoor temperature impacts maximum PCE. The largest effect is observed in low VLT absorbers. The maximum PCE varies by 1.1% between summer and winter for optically-dense (S–Q limit) absorbers. The effect of temperature tapers off as VLT increases, and seasonal differences nearly disappear for VLT > 0.6.

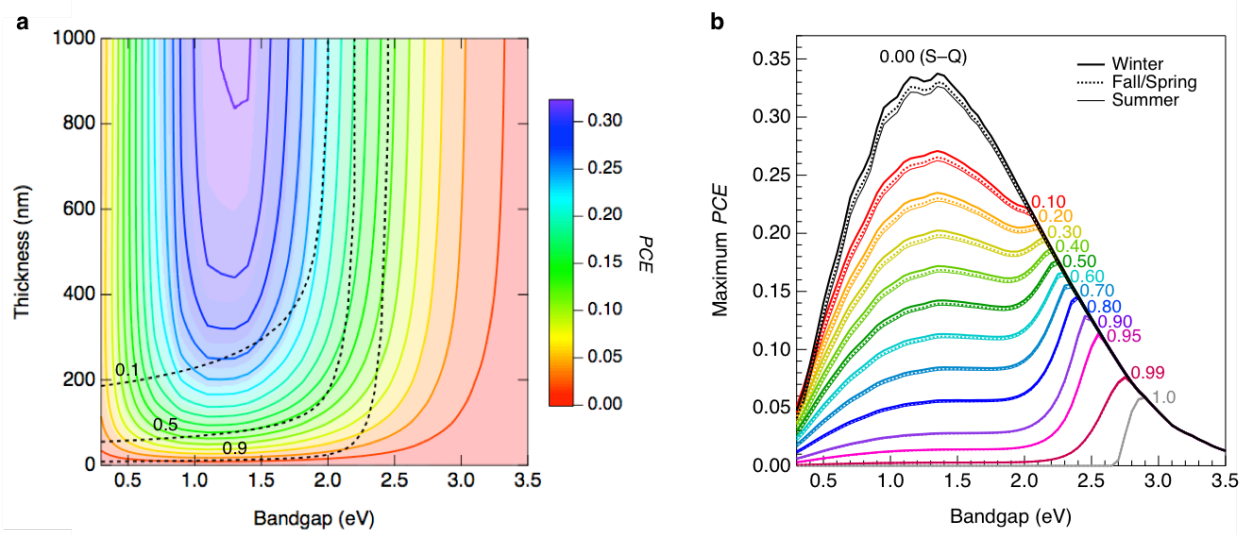

Figure 2. (**a**) Contour plot of the PCE as a function of absorber thickness and bandgap. The dashed black curves are lines of constant VLT = 0.1, 0.5, and 0.9 where the absorber thickness has been optimized for maximum PCE. (**b**) Maximum PCE as a function of bandgap. The set of black curves assumes an optically-dense film to approximate the S–Q limit for each climate condition considered. Each set of colored curves are calculated at constant VLT, indicated by the corresponding label.

The most striking observation from Fig. 2b is the trend in ideal bandgap for maximum PCE as VLT increases. It is a drastic deviation from the S–Q limit. The trend reveals two distinct regimes (Fig. 3). The first regime is characterized by low-VLT (<0.3) and a bandgap between 1 and 1.5 eV with a peak at 1.35 eV. This regime is consistent with the S–Q limit[17], so conventional PV absorbers fall into this regime: α-Si (E_{Gap}=1.5 eV),

CIGS (E_{Gap}=1.0–1.7 eV), CdTe (E_{Gap}=1.5 eV), CZTS (E_{Gap}=1.4–1.5 eV). The conventional absorbers may be thinned to achieve $VLT \leq 0.3$ without sacrificing maximum theoretical PCE. 2) A second high-VLT regime ($VLT > 0.3$) exists in which the ideal bandgap for maximum PCE increases monotonically from 2 to 3 eV with increasing VLT. Maximum PCE decreases from 0.20 to 0.05 for bandgaps of 2 and 3 eV, respectively (Fig. 3a). A fully transparent device that converts UV photons only is thus theoretically limited to 5% PCE. Recent work has shown this limit may be approached in practice[27] and may provide enough converted energy to power an electrochromic device[28].

The distinct VLT regimes have not been identified previously and represent a new design criterion for PV windows. A high-VLT device will have a higher theoretical PCE employing absorbers with larger bandgaps than when thinned conventional absorbers are used. This observation motivates the development of window PV-specific absorbers. The metal halide perovskite family of materials are an obvious fit, as their bandgap is easily tuned using halide anion composition[29] and can be fabricated over large areas in a fashion compatible with glazing manurfacturing[30].

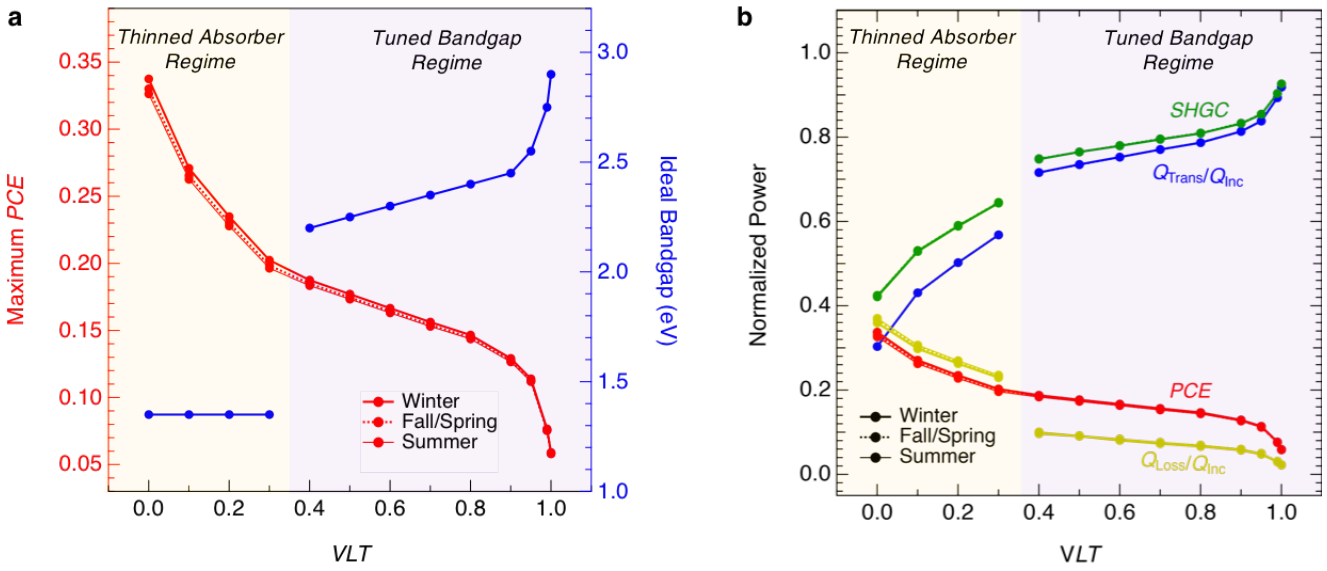

Figure 3. (**a**) Maximum PCE (left axis) and ideal bandgap (right axis) as a function of VLT. (**b**) Normalized power as a function of VLT. Thick, dashed, and thin lines represent winter, fall/spring, and summer conditions, respectively. The seasonal differences in **b** are shown but negligible.

The shift from the thinned absorber regime to the tuned bandgap regime has consequences outside of PCE as shown in Fig. 3b, plotting normalized power as a function of VLT. Whereas PCE (red) shows a smooth decrease as VLT increases, there are sharp changes at the transition point for the other components of the window PV energy balance given by Eq. 6 and 7—fraction of power lost (gold), fraction of power transmitted (blue), and $SHGC$ (green). $SHGC$ and the fraction of transmitted power intuitively trend together. The fraction of power lost within the cell shows a sharp change at the transition from one regime to the next; thermalization is decreased since fewer photons are absorbed as the bandgap is increased.

Thermal performance of PV windows is an underappreciated attribute of the device, with the exception of limited examples[31]. The overall energy balance as a function of bandgap (with absorber thickness optimized for maximum PCE) is further explored in Fig. 4 by plotting the terms in Eq. 6 and 7. The fraction of power that is transmitted includes any visible light transmitted and always contributes to solar $SHGC$ (vertical hash). The energy lost in the cell and transferred into the building (horizontal hash) also contributes to $SHGC$ with varying degrees, depending on the bandgap.

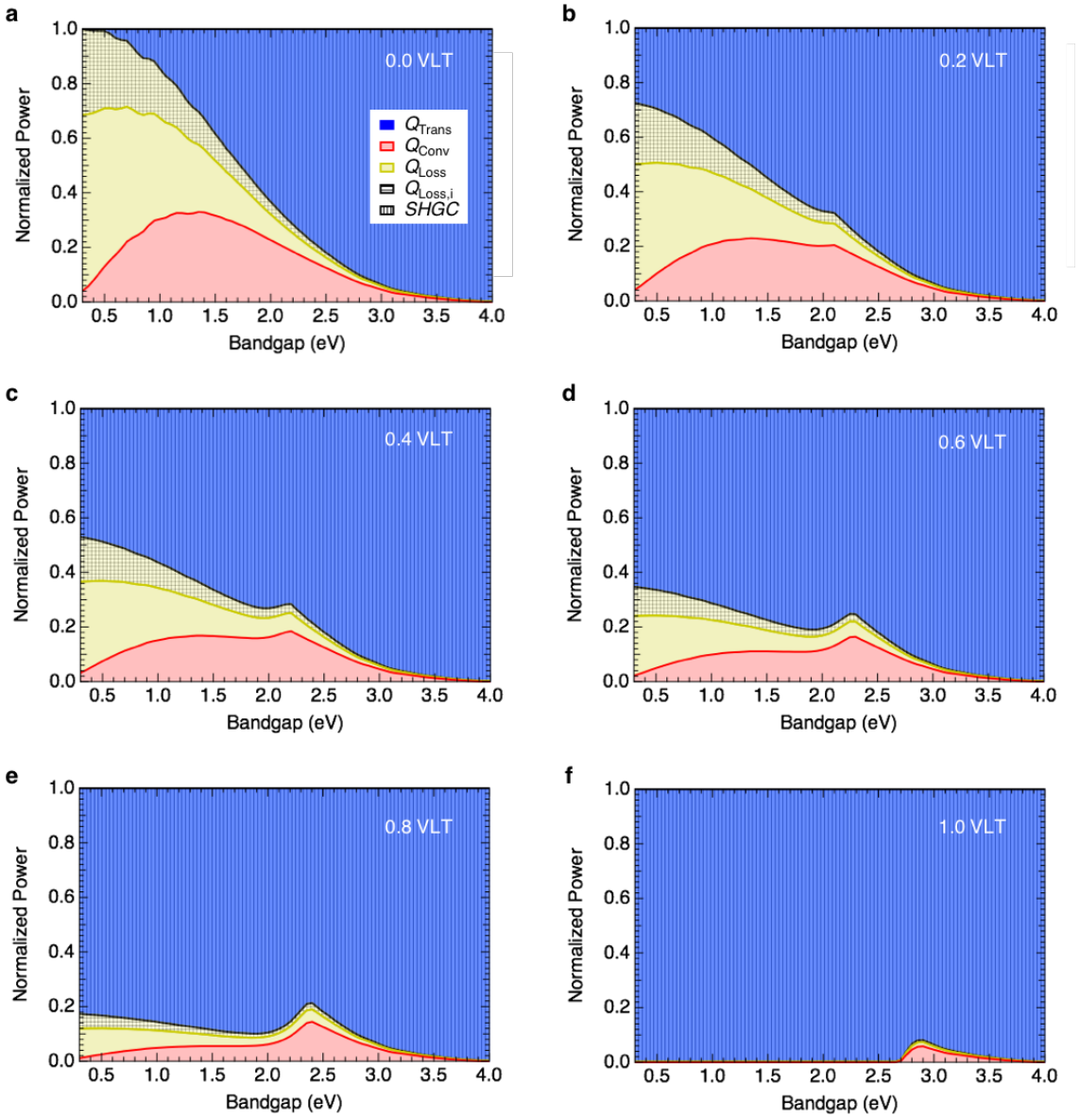

Figure 4. Breakdown of normalized power as a function of bandgap for a constant VLT of 0.0 **(a)**, 0.2 **(b)**, 0.4 **(c)**, 0.6 **(d)**, 0.8 **(e)**, and 1.0 **(f)**. Contributions are broken down into power transmitted through the window (blue), power absorbed and lost in the cell (yellow), and power converted into electricity (red). Hashed regions represent power contributions to solar heat gain (vertical hash) and power lost in the cell that is transferred into the building (vertical hash). Fall conditions are assumed where $Q_{\Delta T} = 0$.

The impact of $Q_{\mathrm{Loss},i}$ depends on practical deployment. Here we assumed a window with zero thermal resistance and a heat transfer coefficient at both sides of the cell. However, if the PV device were on the outside pane of a highly-insulating double-pane, triple-pane, or vacuum-insulating window, then the heat transfer to the inside would be largely stifled, as $U_{\mathrm{o}} \gg U_{\mathrm{i}}$, and most of the energy would be transferred outside. The opposite is true if the PV device is on the inside of a multi-pane window: a larger portion of the power lost in the cell would transfer to the building. Essentially, Q_{Loss} may transfer inside, outside, or both, depending on the position of the PV device, which changes U_{i} and U_{o}. The assumption made here of a window with zero thermal resistance only has the consequence of shifting $Q_{\mathrm{Loss,i}}$ within Q_{Loss}; the fraction of light converted, transmitted, or lost is not affected. The impact of Q_{Loss} on $SHGC$ is most dominant at low$-VLT$ and narrow bandgap, as seen for an opaque cell (VLT = 0.0, Fig. 4a) or cells in the thinned absorber regime (Fig. 4b). $SHGC$ is dominated by transmitted light in the tuned-bandgap regime, especially at the ideal bandgap (Fig. 4c–f).

The final consideration in PV window design is the color of the transmitted light[12]. Though control of the color is valuable for ornamental installments, as often done with colorful dye-sensitized solar cells, the most commonly desired architectural aesthetic is neutral gray. The color of transmitted light for cells with bandgaps between 0.3 eV and 3.5 eV with varied thickness encompass a distinct space on the CIE chromaticity diagram that spans shades of yellow, orange, and red (Fig. 5a, grayed region). The neutral color position occurs at (x, y)=(0.33, 0.34). The maximum PCE for different VLT values are superposed on Fig. 5a. Neutral gray is never achieved for the direct bandgap-like absorbers simulated here, even for absorbers with sub-maximum PCE.

Coloration for each VLT is better visualized by plotting CIE x and y components as a function of bandgap (Figs. 5b and c). Coloration is less dramatic for ideal bandgap absorbers (black markers) in the thinned absorber regime ($VLT \leq 0.3$) but exhibit hues of orange and red as the bandgap is increased to greater-than-ideal values. In contrast, ideal bandgap absorbers in the tuned bandgap regime $VLT > 0.3$ are highly colored and trend from orange to yellow as VLT increases. Patterning the absorber at the microscale has been shown to yield a neutral gray, semitransparent device.[32] Color filtering layers may be added to the PV device stack to achieve a neutral or desired color.[33] A color filter would not affect PCE since it can be placed behind the absorber, but color filters will certainly decrease VLT and $SHGC$, as the amount of transmitted light will decrease.

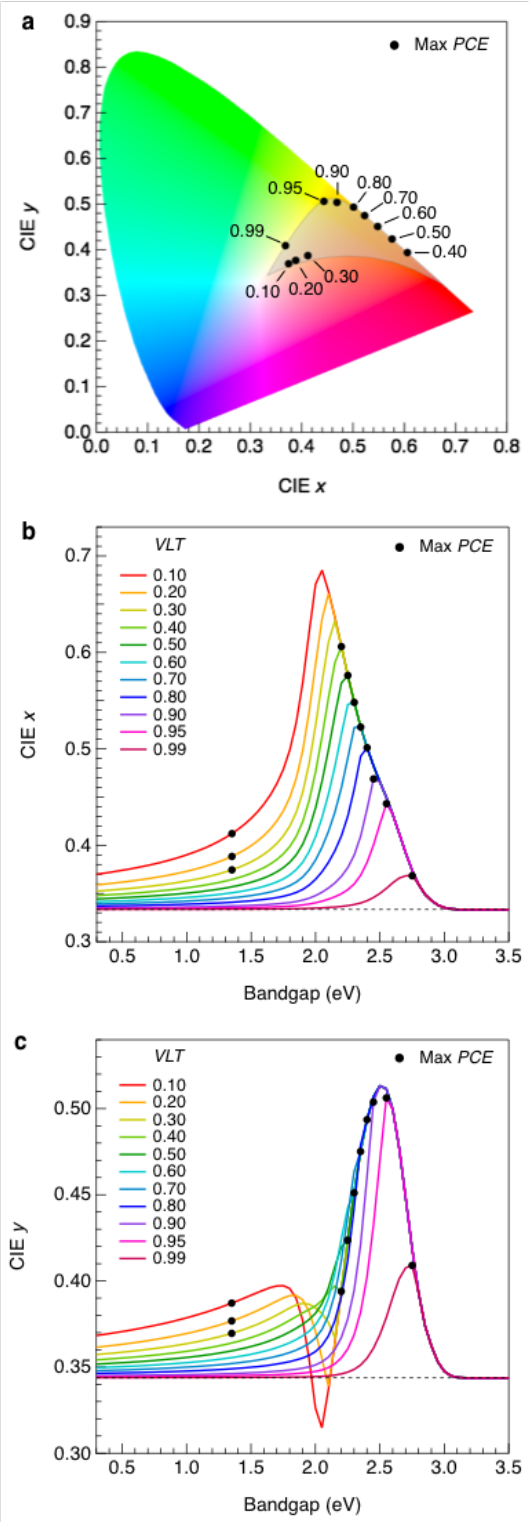

Figure 5. (**a**) CIE chromaticity diagram showing the color of PV windows with bandgaps between 0.3 eV and 4 eV (grayed region). Maximum PCE for a variety of VLT are marked with labels. (**b**) x- and **(c)** y-coordinate of the CIE chromaticity as a function of absorber bandgap at constant VLT. Black markers indicate bandgap with maximum PCE for each VLT. Neutral gray values for x and y are shown as dashed horizontal lines. Window temperature (T_{Cell}) does not significantly affect color.

Conclusion

The enormous potential of PV windows to transform the energy landscape must be reconciled with the fundamental design of the PV window device. Here we developed a detailed balance analysis of PV windows in order to investigate the major design elements of PCE, VLT, $SHGC$, and color. We discovered two distinct regimes of PV absorber design. The thinned-absorber regime validates the common approach to semitransparent PV windows where conventional absorber materials (Si, CIGS, CdTe, CZTS, perovskite, etc.) with an ideal bandgap between 1.1 and 1.5 eV are thinned to allow visible light to pass through. The second, tuned bandgap regime, was unrecognized before this work. The ideal bandgap for maximum PCE in this regime increases monotonically from 2 to 3 eV with increasing VLT. The solar cell exhibits lower losses, higher $SHGC$, and color that trends from yellow to orange and red. Solar cell design elements are strongly coupled together. Moving from a static absorber to the recent discovery of switchable ones[34-36] reduces the constraints described here to allow for more independent control over PCE, VLT, and $SHGC$ to offer even greater potential in high efficiency and greater building energy savings in the future of the built environment.

Acknowledgements

This work was authored by the National Renewable Energy Laboratory, operated by Alliance for Sustainable Energy, LLC, for the U.S. Department of Energy (DOE) under Contract No. DE-AC36-08GO28308. Funding provided by the Building Technologies Offices within the U.S. Department of Energy Office of Energy Efficiency and Renewable Energy. The views expressed in the article do not necessarily represent the views of the DOE or the U.S. Government. The U.S. Government retains and the publisher, by accepting the article for publication, acknowledges that the U.S. Government retains a nonexclusive, paid-up, irrevocable, worldwide license to publish or reproduce the published form of this work, or allow others to do so, for U.S. Government purposes. The authors thank Giles Eperon (NREL) for insight and Steven Byrnes (http://sjbyrnes.com) for writing the original code from which these calculations were adapted.

References

1. Seto, K. C. *et al. Human Settlements, Infrastructure and Spactial planning*. *Climate Change 2014: Mitigation of Climate Change, Contribution of Working Group III to the Fifth Assessment Report of the Intergovernmental Panel on Climate Change,* 923–1000 (2014).
2. United Nations, Department of Economic and Social Affairs, Population Division. *World Urbanization Prospects: The 2014 Revision*. 1–517 (2015).
3. Güneralp, B. *et al.* Global scenarios of urban density and its impacts on building energy use through 2050. *Proc. Natl. Acad. Sci. U.S.A.* **114,** 8945–8950 (2017).
4. Benemann, J., Chehab, O. & Schaar-Gabriel, E. Building-integrated PV modules. *Sol. Energy Mater Sol. Cells* **67,** 345–354 (2001).
5. Kurtz, S. *et al.* Solar research not finished. *Nat Photon* **10,** 141–142
6. Wilson, A. Rethinking the All-Glass Building. *Building Green* **19,** (2010).
7. Cannavale, A. *et al.* Forthcoming Perspectives of Photoelectrochromic Devices: A critical review. *Energy & Environmental Science* **9,** 2682–2719 (2016).

8. Traverse, C. J., Pandey, R., Barr, M. C. & Lunt, R. R. Emergence of highly transparent photovoltaics for distributed applications. *Nat. Energy* 1–12 (2017).
9. Lunt, R. R. Theoretical limits for visibly transparent photovoltaics. *Appl. Phys. Lett.* **101,** 043902 (2012).
10. Lunt, R. R., Osedach, T. P., Brown, P. R., Rowehl, J. A. & Bulović, V. Practical Roadmap and Limits to Nanostructured Photovoltaics. *Adv. Mater.* **23,** 5712–5727 (2011).
11. Chen, C.-C. *et al.* Visibly Transparent Polymer Solar Cells Produced by Solution Processing. *ACS Nano* **6,** 7185–7190 (2012).
12. Forberich, K., Guo, F., Bronnbauer, C. & Brabec, C. J. Efficiency Limits and Color of Semitransparent Organic Solar Cells for Application in Building-Integrated Photovoltaics. *Energy Technology* **3,** 1051–1058 (2015).
13. Tai, Q. & Yan, F. Emerging Semitransparent Solar Cells: Materials and Device Design. *Adv. Mater.* **29,** 1700192 (2017).
14. Sun, J. & Jasieniak, J. J. Semi-transparent solar cells. *Journal of Physics D: Applied Physics* **50,** 093001–29 (2017).
15. Debije, M. G. & Verbunt, P. P. C. Thirty Years of Luminescent Solar Concentrator Research: Solar Energy for the Built Environment. *Advanced Energy Materials* **2,** 12–35 (2011).
16. Treml, B. E. & Hanrath, T. Quantitative Framework for Evaluating Semitransparent Photovoltaic Windows. *ACS Energy Lett.* **1,** 391–394 (2016).
17. Shockley, W. & Queisser, H. J. Detailed Balance Limit of Efficiency of p-n Junction Solar Cells. *J. Appl. Phys.* **32,** 510–519 (1961).
18. Nozawa, T. & Arakawa, Y. Detailed balance limit of the efficiency of multilevel intermediate band solar cells. *Appl. Phys. Lett.* **98,** 171108 (2011).
19. Xu, Y., Gong, T. & Munday, J. N. The generalized Shockley-Queisser limit for nanostructured solar cells. *Sci. Rep.* **5,** 13536 (2015).
20. Datas, A. & Algora, C. Detailed balance analysis of solar thermophotovoltaic systems made up of single junction photovoltaic cells and broadband thermal emitters. *Sol. Energy Mater Sol. Cells* **94,** 2137–2147 (2010).
21. Sha, W. E. I., Ren, X., Chen, L. & Choy, W. C. H. The efficiency limit of $CH_3NH_3PbI_3$ perovskite solar cells. *Appl. Phys. Lett.* **106,** 221104 (2015).
22. Hanna, M. C. & Nozik, A. J. Solar conversion efficiency of photovoltaic and photoelectrolysis cells with carrier multiplication absorbers. *J. Appl. Phys.* **100,** 074510 (2006).
23. Antonopoulos, K. A. & Valsamakis, S. P. Effects of indoor and outdoor heat-transfer coefficients and solar absorptance on heat flow through walls. *Energy* **18,** 259–271 (1993).
24. Schubert, E. F. & Kim, J. K. Solid-state light sources getting smart. *Science* (2005).
25. Chen, B. *et al.* Efficient Semitransparent Perovskite Solar Cells for 23.0%-Efficiency Perovskite/Silicon Four-Terminal Tandem Cells. *Advanced Energy Materials* **6,** 1601128 (2016).
26. Zhao, Y., Meek, G. A., Levine, B. G. & Lunt, R. R. Near-Infrared Harvesting Transparent Luminescent Solar Concentrators. *Advanced Optical Materials* **2,** 606–611 (2014).

27. Liu, D., Yang, C. & Lunt, R. R. Halide Perovskites for Selective Ultraviolet-Harvesting Transparent Photovoltaics. *Joule* 1–12 (2018).
28. Davy, N. C. *et al.* Pairing of near-ultraviolet solar cells with electrochromic windows for smart management of the solar spectrum. *Nat. Energy* **2,** 17104–10 (2017).
29. McMeekin, D. P. *et al.* A mixed-cation lead mixed-halide perovskite absorber for tandem solar cells. *Science* **351,** 151–155 (2016).
30. Dou, B. *et al.* Roll-to-Roll Printing of Perovskite Solar Cells. *ACS Energy Lett.* acsenergylett.8b01556 (2018).
31. Sun, C. *et al.* Heat-Insulating Multifunctional Semitransparent Polymer Solar Cells. *Joule* **2,** 1816–1826 (2018).
32. Eperon, G. E., Burlakov, V. M., Goriely, A. & Snaith, H. J. Neutral Color Semitransparent Microstructured Perovskite Solar Cells. *ACS Nano* **8,** 591–598 (2014).
33. Wen, L. *et al.* Theoretical design of multi-colored semi-transparent organic solar cells with both efficient color filtering and light harvesting. *Sci. Rep.* **4,** 7036 (2014).
34. Wheeler, L. M. *et al.* Switchable photovoltaic windows enabled by reversible photothermal complex dissociation from methylammonium lead iodide. *Nat. Commun.* **8,** 1722 (2017).
35. Lin, J. *et al.* Thermochromic halide perovskite solar cells. *Nat Mater* 1–9 (2018).
36. Goldschmidt, J. C. From window to solar cell and back. *Nat Mater* **17,** 218–219 (2018).